IEEE Access
Multidisciplinary | Rapid Review | Open Access Journal

Received 23 January 2024, accepted 21 February 2024, date of publication 29 February 2024, date of current version 12 March 2024.

Digital Object Identifier 10.1109/ACCESS.2024.3371701

RESEARCH ARTICLE

High-Directivity and Low-Loss Directional Couplers Based on Empty Substrate Integrated Coaxial Line Technology

DAVID HERRAIZ[1], (Graduate Student Member, IEEE), HÉCTOR ESTEBAN[1], (Senior Member, IEEE), DARÍO HERRAIZ[2], JUAN J. DE DIOS[2], MARCOS D. FERNANDEZ[2], ANGEL BELENGUER[2], (Senior Member, IEEE), AND VICENTE E. BORIA[1], (Fellow, IEEE)

[1]Instituto de Telecomunicaciones y Aplicaciones Multimedia, Universitat Politècnica de València, 46022 Valencia, Spain
[2]Departamento de Ingeniería Eléctrica, Electrónica, Automática y Comunicaciones, Escuela Politécnica de Cuenca, Universidad de Castilla-La Mancha, 16071 Cuenca, Spain

Corresponding author: David Herraiz (daherza@teleco.upv.es)

This work was supported in part by MCIN/AEI/10.13039/501100011033, Spanish Government, under the Coordinated Research Project, through Subprojects C41 and C44, under Grant PID2022-136590OB; in part by MCIN/AEI/10.13039/501100011033, Spanish Government; and in part by the European Union Next Generation European Union/Plan de Recuperación, Transformación y Resiliencia (EU/PRTR), under the Coordinated Research Project, through Subprojects C41 and C44, under Grant TED2021-129196B.

ABSTRACT High-directivity and low-loss directional couplers based on Empty Substrate Integrated Coaxial Line (ESICL) technology are presented in this article. The proposed coupled line directional couplers are based on the combination of a high-isolation section, a tapered transition based on splines between the access lines and the high-isolation sections, coupled lines of reduced width and inclined arms. The design evolution has justified the combination and precise adjustment of these elements, proving to be a solution to increase directivity, improve return losses and achieve a more stable coupling coefficient. The use of ESICL technology shows great promise in terms of electrical performance, bandwidth, seamless integration with other planar circuits and ease of manufacture. For comparison, two directional couplers with the same coupling coefficient but different operating frequencies have been designed and fabricated. A microstrip coupler was also designed and fabricated for comparison. The simulated and measured results clearly show that the ESICL directional couplers outperform their microstrip counterparts in terms of losses and directivity, without the need for additional lumped elements or complex geometries.

INDEX TERMS Empty substrate integrated coaxial line, directional couplers, transition, substrate integrated circuit, tapering structure, high-directivity.

I. INTRODUCTION

The operating frequency of the satellite communications industry reveals a growing trend, moving towards the Ku, K, and Ka frequency bands [1]. This interest arises from the new communications system requirements, in particular particularly for emerging satellite communications systems based on small satellites, picosatellites, or nanosatellites, which require higher bandwidth and throughput levels. This technological trend, while unable to entirely replace conventional satellite systems based on large satellites, introduces new paradigms in the development of novel and compact technological solutions. Consequently, microwave engineers are faced with the challenged to develop passive components and equipment, such as filters, diplexers, antennas, and others, that strike a balance between electrical performance requirements with volume, weight, and manufacturing costs

Conventional communication satellite systems usually employ a payload implemented with waveguide technology, at least for the output stage. These components offer

The associate editor coordinating the review of this manuscript and approving it for publication was Qi Luo.

high-quality electrical performance, high power-handling capabilities, and mechanical robustness [2]. However, they have significant drawbacks, including being bulky, heavy, expensive, and challenges while integrating other technologies. As an alternative, planar technologies, such as microstrip, coplanar, or stripline, provide light-weight, low-volume, cost-effective components that can be easily integrated. Nevertheless, they exhibit higher insertion loss, which can lead to insufficient electrical performance for some applications. Consequently, a gap exists between waveguide and planar technologies that needs to be addressed. In this context, substrate integrated technologies, particularly the Empty Substrate Integrated Coaxial Line (ESICL) [3], offer a hybrid solution that combines the advantages of both planar and coaxial line technologies.

A coupled line coupler is one of the most common building blocks used in many microwave and millimetre-wave systems, playing a critical role as a power divider or combiner in mixers, modulators and antenna feed networks [4]. Traditionally, coupled line couplers are designed using planar technologies because of their ease of integration and fabrication [4]. However, microstrip couplers suffer from crosstalk, radiation losses and high insertion losses due to their unshielded structure. They also have poor isolation and poor directivity due to the difference in phase velocities between even and odd modes [5]. The directivity is limited to only 20 dB for microstrip couplers [4]. Many solutions have been proposed to improve directivity, such as the use of additional lumped elements [6], [7], dielectric overlays [8] and wiggling lines [9]. These devices have been experimentally verified for their high directivity characteristics, but they suffer from the same problems as the unshielded structure. In addition, the operating bandwidth of the directivity is narrow; for example, in [6] and [7] the directivity is greater than 20 dB only in a 28% fractional bandwidth and requires additional lumped elements such as capacitors. A good candidate to solve the problems of external noise and radiation losses is the Substrate Integrated Coaxial Line (SICL) [10], in which the arrays of vias act as a lateral shield to prevent the propagation of unwanted parallel plate modes. Several microwave components have been developed using SICL [11], [12], [13], [14], and this technology has also been used to design low frequency directional couplers, as reported in [15], [16], and [17]. However, directional couplers up to 6 GHz have not been developed in SICL due to the propagation of the electromagnetic wave through the dielectric medium, which leads to increased insertion losses at higher frequencies (above 6 GHz). Therefore, to improve the directivity, bandwidth and insertion loss of directional couplers, the Empty SICL [3] is the most suitable technology, which avoids leakage and at the same time provides low insertion loss due to the absence of dielectric.

Therefore, this article proposes a new directional coupler based on coupled lines in ESICL technology. The presented structure provides high isolation, good coupling level and higher operating bandwidth. The paper is organised as follows. Section II, introduces the ESICL structure and the basic theory of directional couplers based on this technology. The proposed structure and its development, together with the effect of the main parameters and the design procedure, are presented in Section III. In Section IV, broadband directional couplers are designed at several frequencies, and then two prototypes are fabricated and measured. Performance comparisons with other designs in ESICL and microstrip technologies are also given. Finally, the conclusions are presented and discussed in section V.

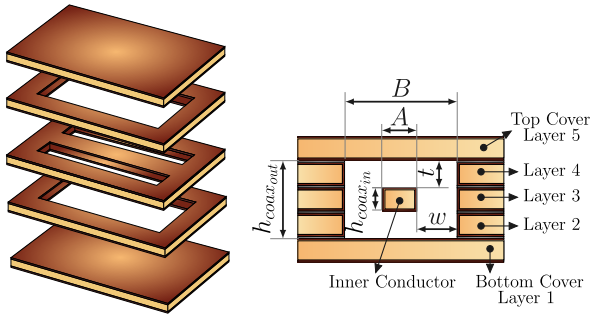

(a) 3D view of piled layers (b) ESICL transversal section

FIGURE 1. Structure of the empty substrate integrated coaxial line.

II. ESICL

A. TRANSVERSAL SECTION DESIGN

In the pursuit of integrating the traditional 3D waveguide into a planar substrate, the concept of Substrate Integrated Waveguide (SIW) has been introduced. SIW consists of a waveguide manufactured on a substrate using two rows of metalized via holes, as described in [18]. A coaxial version, named Substrate Integrated Coaxial Line (SICL) [10], has been also developed using two stacked printed circuit boards. In SICL, the inner conductor is created using a metal strip, while the outer conductor is formed by two lateral rows of metallic via holes in each layer and the top and bottom layers. Unfortunately, both SIW and SICL suffer from the problem of wave propagation through the dielectric medium of the substrate, resulting in high insertion losses at higher frequencies. Consequently, their performance is compromised. To enhance electrical performance, a variation called Empty SIW (ESIW) was introduced [19]. In ESIW, the dielectric is removed, resulting in transmission lines that are better suited for higher frequencies with lower insertion losses. Similarly, an Empty SICL (ESICL) has been developed [3]. ESICL is essentially an empty coaxial line integrated into a stack of five layers of PCB, as depicted in Fig. 1. The active conductor is implemented in the third layer, while the outer conductor of the coaxial line is constructed using the first and fifth layers. The inner and outer conductors are separated both vertically and horizontally in layers two and four.

Similar to a coaxial line, the ESICL is a non-dispersive transmission line, meaning that its first mode of propagation is the transverse electromagnetic mode (TEM).

Additionally, ESICL has very low transmission and radiation losses while maintaining the cost efficiency of planar technologies. Thanks to these exceptional advantages, several high-performance components have been developed, including filters [20], [21], [22], transitions to grounded coplanar and microstrip lines [19], [23], power dividers [24], [25] and circulators [26]. However, no directional couplers have yet been designed using this novel technology. To design a directional coupler, it is crucial to determine the physical dimensions that control the monomode frequency range and characteristic impedance. We consider the total height of the ESICL as a fixed parameter, which depends on the commercial substrate thickness (h_s) and the metallisation thickness with copper deposition (m). Therefore, the total height of the ESICL is given by $h_{coax_{out}} = 3h_s + 6m$. The height of the inner conductor is also a fixed parameter due to the substrate height h_s used. Consequently, the physical dimensions that control the characteristic impedance are the inner and outer conductor widths, denoted A and B respectively [see Fig. 1(b)].

These widths can be calculated using the Method of Moments (MoM) [27] or closed-form expressions [28] over the ESICL cross-section. The MoM method provides higher accuracy but requires longer simulation times, in contrast to the closed expressions, which offer shorter simulation times with lower accuracy. In this study, the MoM method was used to calculate the coaxial characteristic impedance. The monomode frequency range for a TEM mode in ESICL extends from DC to the cutoff frequency at which higher order modes are propagated. In ESICL, the first high order mode is either TE_{10} or TE_{01}, and its cut-off frequency f_c can be calculated using the following expressions for the TE_{10} [29],

$$\cot\left(\frac{2\pi t f_c}{c}\right) - \tan\left(\frac{h_{coax_{in}}\pi f_c}{c}\right) = \frac{B_r}{Y_r} \tag{1}$$

where c is the light velocity, f_c the cutoff frequency, and $\frac{B_r}{Y_r}$ the susceptance between the inner and outer conductor, which can be calculated as [30],

$$\frac{B_r}{Y_r} = \frac{2f_c}{c}(h_{coax_{in}} + 2w)\left[-\ln(4u) + \frac{1}{3}u^2 + \frac{1}{2}\left(1-u^2\right)^2\left(\frac{f_c(A+2w)}{c}\right)^2\right] \tag{2}$$

$$u = \frac{2w}{w+A} \tag{3}$$

Solving the Eqs. (1), 2 and (3), the cutoff frequency of the mode TE_{10} can be obtained. For the mode TE_{01}, the equations are the same, but the following changes need to be addressed: $t \to w$, $A \to h_{coax_{in}}$, $w \to t$, and $h_{coax_{in}} \to A$. Note that for a fixed heights $h_{coax_{out}}$ and $h_{coax_{in}}$, a lower value of parameter B will result in a larger monomode range of the TEM mode, as evidenced in [25], but it will increase the complexity in manufacturing.

B. DESIGN OF ESICL DIRECTIONAL COUPLERS

A conventional directional coupler can be created by placing two microstrip lines in close proximity, where their coupling arises from near-field interactions. Although the degree of coupling depends on the length and spacing of these sections, it is difficult to achieve strong coupling by controlling these parameters alone. This often leads to the need for closely spaced lines, resulting in complex manufacturing processes. To achieve a strong coupling, it is possible to enclose the microstrip lines, creating two striplines. This approach can also be applied to the ESICL, taking advantage of its low losses due to dielectric removal.

The length of the coupled section is fixed to a one-quarter of a wavelength ($l = \lambda_g/4$) at the operating frequency [31]. Due to the cross-sectional symmetry of this uniform structure, the fields within the coupling section can be described as a superposition of even and odd modes, as explained in [31]. Consequently, the even (Z_o^e) and odd (Z_o^o) impedances of ESICL can be calculated by considering the coupling effect as follows:

$$Z_o^e = Z_d\sqrt{\frac{1+C}{1-C}} \tag{4}$$

$$Z_o^o = Z_d\sqrt{\frac{1-C}{1+C}} \tag{5}$$

where Z_d is the desired characteristic impedance and C is the desired coupling coefficient. Consequently, the even and odd impedances of the coaxial line can be synthesized in ESICL physical dimensions, taking into account that the height is a fixed parameter and the widths are the design parameters to accomplish the desired coupling coefficient and characteristic impedance. Further details and the design procedure for the proposed directional coupler are given in the following sections.

III. REALIZATION OF ESICL DIRECTIONAL COUPLERS

A. STRUCTURE

The first approach of the directional coupler is based on the coupled section connected to the access lines using a 90°bend, as shown in Fig. 2(a), designated ESICL I. However, this configuration provides poor isolation of the adjacent port, leading to a non-competitive directivity at central frequency $D < 10$ dB (see Fig. 13(d) and 12(d)). In order to achieve strong isolation of the adjacent port, and a smooth flow of the electromagnetic wave of the coupling region, a second approach is proposed, as shown in Fig. 2(b), denoted by name ESICL II. This coupler presents three sections; one section corresponds to the access lines, while the central section corresponds to the coupling section, with a reduced size compared to the access lines. Finally, the third section corresponds to the inclined arms, which connect the access lines and the coupled section. The inclined arm presents a transition with a linear profile between the access lines and the reduced coupled section. It can be observed that the main differences between the first (ESICL I) and second (ESICL II) approaches are related to the reduced coupled

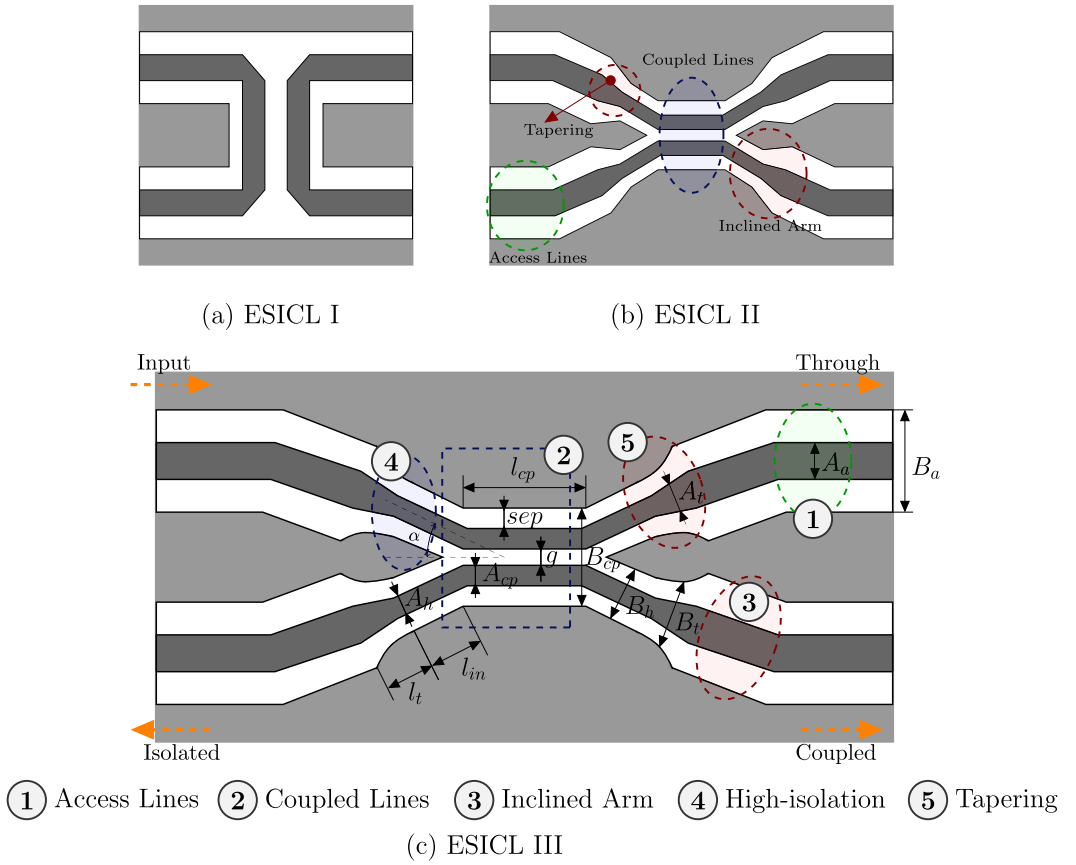

FIGURE 2. Evolution of the proposed directional coupler includes: (a) ESICL I with 90Â° bends, (b) ESICL II with an inclined arm and linear transition, and (c) ESICL III, the final directional coupler with a spline transition, high-isolation section, and inclined arm.

section and the inclined arm with a linear transition profile. An initial value of the most important parameters has been used, as a proof of concept of this topology with the aim to evaluate the performance, resulting in a higher directivity at operation frequency, although when frequency increases, the directivity decreases (see Figs. 13(d) and 12(d)). Therefore, in order to improve the directivity over a wider frequency range, the final directional coupler structure is proposed, referred to as ESICL III, as shown in Fig. 2(c). This directional coupler consists of five sections, access lines (number 1), coupled lines (number 2) with an outer conductor width smaller than the access lines, inclined arms (number 3) to connect both sections, a high isolation section with a reduced outer conductor width (number 4) to enhance the isolation, and a tapered section (number 5) to ensure constant impedance, thereby improving the reflection coefficient. In the following subsections, the differences between the previously proposed directional couplers (ESICL I and II) and the influence of the design parameters on their performance are discussed. For the implementation of the designed ESICL, a ROGERS 4003C substrate with a permittivity constant of $\epsilon_r = 3.55$ and a height of $h_s = 0.813$ mm was chosen for all layers. In this case, the width of the outer conductor for the access lines was set to $B_a = 6$ mm, covering the monomode frequency range from DC to 21.5 GHz.

B. TAPERING SECTION

The second approach of the directional coupler (ESICL II) (see Fig. 2(b)) presents a linear tapering section in the arms, which serves as an impedance transformer between the characteristic impedance of the access lines (B_a and A_a) with a larger cross-section and the reduced section of the coupled lines (B_h and A_h) (see Fig. 3). Although, the initial and final points ensure the same characteristic impedance, a linear taper does not maintain the same characteristic impedance along the entire length of the linear transition. Thus, the points P_1 and P_3 in Fig. 3 a) present the same characteristic impedance; however, the point P_{2l} presents other characteristic impedance, resulting in degraded return losses. Therefore, to ensure a constant characteristic impedance along the transition and improve impedance matching, the linear equation has been replaced by an interpolation method in the proposed directional coupler, as shown in Fig. 2(c). In this case, the inner conductor width (A_t) has been maintained as a linear profile, as depicted in Fig.3b, while the outer conductor width (B_t) has been

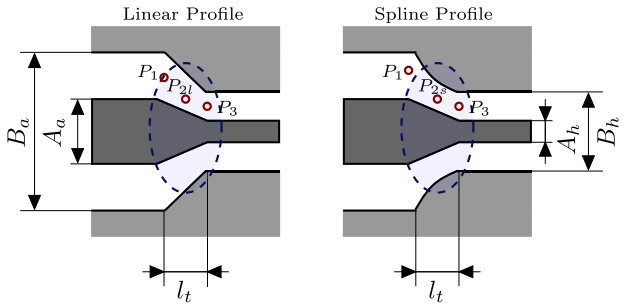

FIGURE 3. ESICL transversal section of the profile transitions.

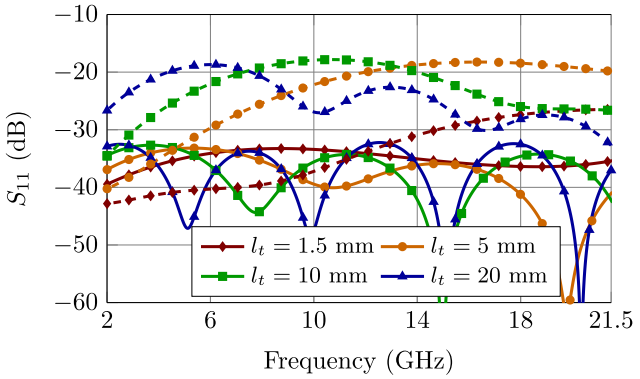

FIGURE 4. Return loss (S_{11}) comparison between spline and linear profiles for different values of transition lengths (l_t). Dashed lines correspond to linear profile and solid lines correspond to spline profile.

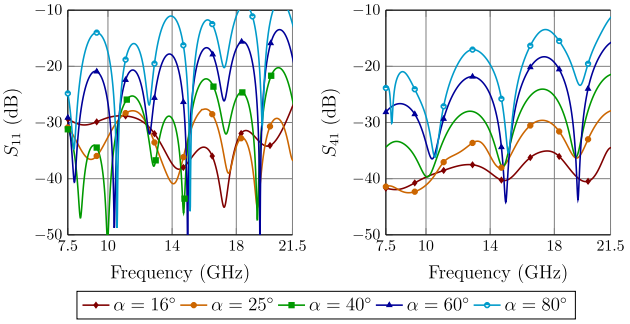

FIGURE 5. Variation of return losses (S_{11}) and isolation (S_{41}) for different values of the angle arm (α).

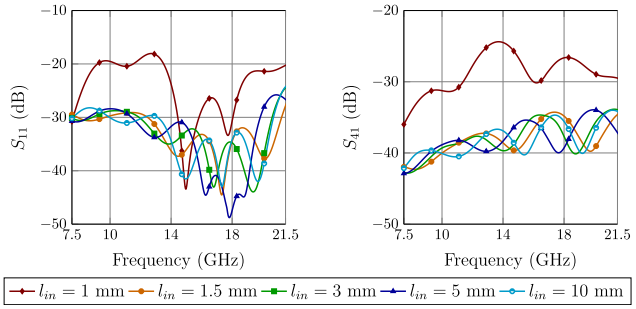

FIGURE 6. Variation of return losses (S_{11}) and isolation (S_{41}) for different values of l_{in}.

adjusted to follow a spline profile [32], [33], [34]. The cross-section view of both transitions is illustrated in Fig. 3.

Figure 4 shows a comparison of S_{11} between both profiles depicted in Fig. 3(a), with $B_a = 6$ mm, $A_a = 1.75$ mm, $B_h = 2$ mm, and $A_h = 0.89$ mm, for different transition lengths (l_t). The linear profile is represented by a dashed line, while the spline profile is shown as a solid line. The inner conductor widths have been calculated to achieve a characteristic impedance of $Z_0 = 50\ \Omega$. It can be seen that the spline profile achieves better return loss than the linear profile over the entire bandwidth, even for small values of the transition length. After designing the directional coupler for multiple frequencies and coupling coefficients, taking into account the entire structure, a good initial approximation for the length of the proposed transition is $l_t = \lambda_g/2$.

C. ANGLE AND INPUT LENGTH ARM

The arm angle (α) (See Fig. 2(c)) is an important parameter affecting the performance of the directional coupler, with significant implications for isolation and return losses. On the one hand, a higher value of the angle parameter approaching 90°degrees results in poor isolation. Conversely, lower values of the angle parameter, nearing the limit at which adjacent conductors collide, result in better isolation. However, a lower angle value reduces the spacing between the conductors, increasing manufacturing complexity. A parametric analysis was conducted to assess the effect of the angle α on the performance of the directional coupler. Fig. 5 illustrates the return losses and isolation of the proposed directional coupler, highlighting the significant influence of the arm angle on these couplers parameters. As expected, higher values of α yield in poor isolation and return losses, while lower values of α, near the fabrication limit, result in better isolation and return losses. It is evident that poor isolation negatively affects the overall directivity of the design. Taking these considerations into account, the optimum compromise between simplicity, ease of manufacture and performance is to set the angle values between 16° and 26°or 25° degrees.

Regarding the length of the input section in the coupled lines, denoted as l_{in} (see Fig. 2(c)), a parametric analysis has been performed in order to evaluate the effect in the directional coupler, as shown in Fig. 6. It can be observed that when $l_{in} = 1$ mm both return losses and isolation suffer a significant degradation, compared to other values of l_{in}, which provides better performance. Notably, higher values of l_{in}, such as 5 mm or 10 mm do not provide better performance than lower values, and have the disadvantage of increased dimensions. Therefore, a suitable initial value for this length is $l_{in} = 1.5$ mm.

D. COUPLED LINES AND HIGH-ISOLATION SECTION

The inner and outer conductor widths (B_h and A_h) of the high-isolation section affect the isolation performance, and consequently, the directivity. A smaller outer conductor width of the ESICL (B_h) enhances isolation, albeit at the cost of increased manufacturing complexity due to the necessity of reducing the inner conductor width (A_h) to maintain the same characteristic impedance. On the other hand, wider widths result in lower isolation. To illustrate the effect of

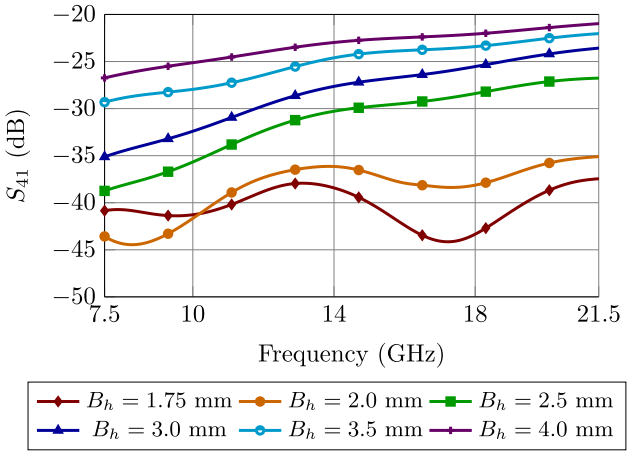

FIGURE 7. Variation of isolation (S_{41}) for different values of B_h.

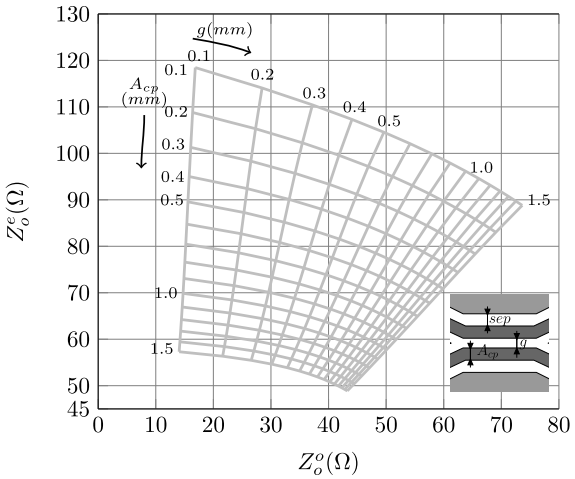

FIGURE 8. Variations of the modal characteristics impedances excitation versus inner conductor width A_{cp} and the distance g for the case sep = 0.5 mm.

reduced width (B_h) on the isolation of the directional coupler, a dimensional analysis was conducted as depicted in Fig. 7. These curves were obtained while keeping the coupling coefficient and characteristic impedance constant of $Z_0 = 50\,\Omega$ and $C = 10$ dB, respectively. The inner conductor width (A_h) was calculated to maintain the desired characteristic impedance. The results show that smaller values of B_h lead to higher isolation, in contrast to higher values of B_h approaching the access lines value of $B_a = 6$ mm, which results in poor isolation. Considering both, manufacturing ease and isolation, an optimal compromise is achieved by setting B_h to 2 mm.

The coupled lines offer design flexibility since there are three physical parameters: the inner conductor width (A_{cp}), the separation between the inner conductor and the outer conductor (sep), and the separation between the inner conductors (g) (See Fig. 2(c)). To explain the effect of these physical parameters on the coupled lines, we consider separate analysis for odd and even modes. For the even mode, it can be observed a weak influence of the separation (g) on

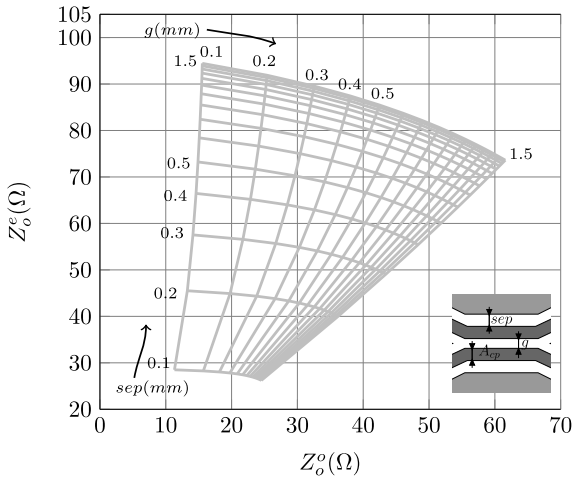

FIGURE 9. Variations of the modal characteristics impedances versus inner conductor width sep and the distance g for the case A_{cp} = 0.89 mm.

the value of Z_o^e. This suggests that the dominant physical parameters determining Z_o^e are the inner conductor width A_{cp} and sep. In contrast, for the odd mode, the separation between the inner conductors (g) has the most significant impact on Z_o^o. These conclusions are validated in Fig. 8, where Z_o^o versus Z_o^e is plotted using A_{cp} and g, while keeping sep constant at 0.5 mm, and in Fig. 9, where Z_o^o versus Z_o^e is plotted using sep and g, while keeping A_{cp} constant at 0.89 mm. These plots reveal that the variation range of Z_o^e when sweeping A_{cp} for a constant g is larger than the reverse case, where g is varied within the same interval while keeping A_{cp} constant (See Fig. 8). This effect is also observed for Z_o^e when sweeping sep for a constant A_{cp} (See Fig. 9). Furthermore, it is apparent that the impact of A_{cp} on the variation range of Z_o^e is more significant than the effect of g. Thus, it can be concluded that Z_o^e is more sensitive to the design parameters sep and A_{cp}, while Z_o^o is primarily influenced by g. To establish an initial starting point, it can be assumed a constant value for $sep = 0.5$ mm since each modal impedance mainly depends on one single parameter ($Z_o^e(A_{cp})$ and $Z_o^o(g)$), leading to the determination of such parameter with the aim to achieve the desired modal impedance value. However, it is essential to note that better performance can be achieved when optimizing all parameters together. Finally, as mentioned before, the length of the coupled section can be considered as $l_{cp} = \lambda_g/4$ at the operation frequency (f_0), although due to the effect of the arms, this length will be lesser and needs to be tuned.

E. DESIGN PROCEDURE

Having explained the effects of the most important physical parameters in the directional coupler, this subsection outlines the procedure for designing the directional coupler, which is summarised in Fig. 10 by means of a step-by-step flowchart.

1) The outer conductor width of the ESICL (B_a) on the access line is calculated to ensure operation at the desired frequency within the monomode frequency

range, accounting for the highest propagation mode using Eq.(1). Subsequently, the inner conductor width (A_a) is calculated using the MoM method to achieve the desired characteristic impedance ($Z_0 = 50\ \Omega$ usually). These dimensions constitute the ESICL access lines.

2) In the high-isolation section, the outer conductor width (B_h) is calculated to balance manufacturing complexity and isolation, as discussed in Section III-D. It is worth noting that a narrower outer conductor width results in smoother electromagnetic wave propagation in the coupling region, leading to higher isolation (more directivity), but at the expense of increased manufacturing complexity. Consequently, it is essential to strike a suitable balance between ease of manufacturing and achieving the desired directivity. Thus, according to Fig. 7, the optimum value is 2 mm. Next, the inner conductor width (A_h) in this section is calculated using MoM to match the previous step characteristic impedance.
3) Next, the impedances Z_o^e and Z_o^o are calculated to obtain the desired coupling coefficient (C) and the characteristic impedance Z_d ($Z_d = Z_0 = 50\ \Omega$) using Eqs. (4) and (5). These modal impedances are then transformed into physical dimensions (g, sep, A_{cp}) using the relationships between the parameters shown in Figs. 8 and 9, which can be obtained using the MoM for other values. This provides an initial point for the main physical parameters in the coupled section.
4) The initial value for the length of the coupled section is set to $l_{cp} = \lambda_g/4$ at the operating frequency. Then the initial value for the transition length l_t is set to $\lambda_g/2$ and the outer conductor width of the transition is calculated using a spline to ensure a constant characteristic impedance. The initial values of l_{in} and α are fixed according to the reasoning explained in Figs. 5 and 6, resulting in the values $l_{in} = 1.5$ mm and $\alpha = 16°$.
5) The final step is an optimization using CST Studio Suite, where all the main physical parameters corresponding to the coupled lines (A_{cp}, sep, g and l_{cp}) and the arm (α, l_t and l_{in}) are tuned simultaneously using a trust region algorithm. This optimization aims to achieve the desired coupling at the operating frequency, minimize input return loss and maximize isolation (and therefore directivity).

IV. DIRECTIONAL COUPLER EXAMPLES AND EXPERIMENTAL RESULTS

A. EXAMPLES

According to the design procedure proposed earlier, several examples of directional couplers are illustrated in this section. Two ESICL-based directional couplers are designed to operate at frequencies of $f_0 = 5$ GHz and $f_0 = 15$ GHz, each with a coupling coefficient of $C = 10$ dB. As mentioned above, the inner conductor width has been determined using eqs. (1) and (2), covering the frequency range from DC to 21.5 GHz, resulting in a value of $B_a = 6$ mm. The inner conductor width is then calculated using the MoM method to give a characteristic impedance of $Z_d = 50\ \Omega$ ($A_a = 1.75$ mm).

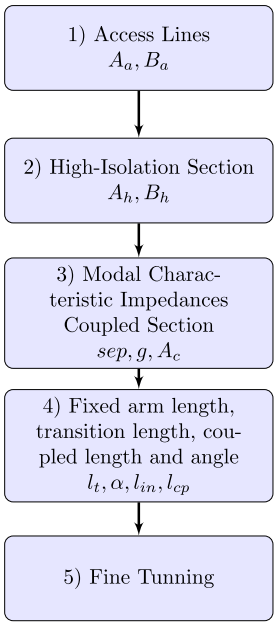

FIGURE 10. Summary of ESICL directional coupler design procedure.

Then, the inner conductor width is calculated using the MoM method to achieve a characteristic impedance of $Z_d = 50\ \Omega$ ($A_a = 1.75$ mm). To enhance isolation over the maximum bandwidth and at the operation frequency, the outer conductor width in the high-isolation section B_h is fixed to $B_h = 2$ mm, and the inner conductor width of this section has been calculated to obtain the same characteristic impedance (Z_d), leading a value of $A_h = 0.89$ mm. Next, the Z_o^e and Z_o^o, have been calculated for the desired coupling coefficient of $C = 10$ dB, and the physical dimensions of the coupled region have been determinated to provide the desired values for the Z_o^e and Z_o^o, leading to the following even and odd impedances $Z_o^e = 69.37\ \Omega$, $Z_o^o = 36.018\ \Omega$, and the following physical dimensions, $sep = 0.5$ mm, $g = 0.45$ mm, and $A_{cp} = 0.88$ mm. The length of the coupled section and the transition were initially set to $l_{cp} = \lambda_g/4 = 5$ mm and $l_t = \lambda_g/2 = 10$ mm at the operation frequency ($f_0 = 15$ GHz). The initial angle value was fixed at the fabrication limit of $\alpha = 16°$, and the value of l_{in} was set at 1.5 mm. Finally, all physical parameters were fine-tuned using CST, applying the objective and algorithm described in step 5 of the design procedure (see III-E). The final values that determine the size of the directional coupler are those included in Table 1. The same method has been applied to the directional coupler at an operating frequency of $f_0 = 5$ GHz, whose initial and final values are included in Table 1. It can be observed that the design procedure yielded values for both directional couplers that were close to the optimized ones.

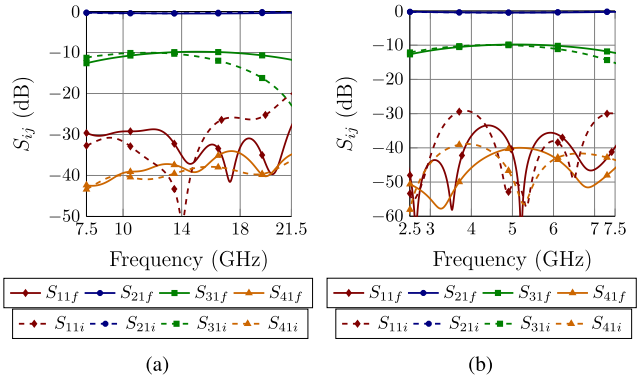

FIGURE 11. Comparison of the initial and final response of the directional coupler at the operation frequency of (a) $f_0 = 15$ GHz, (b) $f_0 = 5$ GHz. Dashed and solid lines correspond to the initial and final points respectively.

TABLE 1. Initial and final values for the design parameters in mm.

$f_0 = 15$ GHz							
	sep	g	A_{cp}	l_{cp}	l_t	l_{in}	α
Initial	0.5	0.45	0.88	5	10	1.5	16°
Final	0.54	0.43	0.87	3.55	9.52	1.45	16.75°
$f_0 = 5$ GHz							
	sep	g	A_{cp}	l_{cp}	l_t	l_{in}	α
Initial	0.5	0.45	0.88	15	30	1.5	16°
Final	0.52	0.43	0.89	13.42	30.78	1.45	17.79°

The initial and final responses of the directional couplers at both frequencies are shown in Fig. 11. It can be seen that the initial point is quite sufficient for the design of the directional coupler and that the initial coupling coefficient achieves the desired value, albeit with a slight frequency shift due to the inclined arms effect.

The final simulated results of the ESICL III directional coupler at both frequencies are compared with the responses of two other directional coupler approaches, referred to as ESICL I (see Fig. 2(a)) and ESICL II (see Fig. 2(c)), together with a conventional microstrip $C = 10$ dB directional coupler at the same operation frequencies in Figs. 12 and 13. Directivity has also been included, once computed from the couplings and isolation at the corresponding frequencies, as shown in Fig. 14. Losses and transitions are not included in these results. Table 2 summarizes the results of the simulated directional couplers in several indexes as minimum level of return losses R_L (dB), the maximum value of insertion losses I_L (dB), the minimum value of isolation I_S (dB), coupling coefficient C (dB) and fractional bandwidth FBW (%) which this coefficient remains stable, and minimum value of directivity D (dB) in the whole frequency band. It can be observed in both operational frequencies that the proposed ESICL III directional coupler achieves better return losses and isolation compared to ESICL II, ESICL I, and microstrip directional couplers. The coupling coefficient remains more stable for the ESICL III and ESICL II directional couplers in comparison to the microstrip and ESICL I directional coupler. The directivity of the ESICL III directional coupler is 6 dB greater than the ESICL II directional coupler, 7 dB greater than the microstrip coupler, and 14 dB greater than the ESICL I directional coupler at an operation frequency of $f_0 = 5$ GHz, while at $f_0 = 15$ GHz, the directivity of the ESICL III directional coupler is 7 dB greater than the ESICL II directional coupler, 13 dB greater than the microstrip coupler, and 21 dB greater than the ESICL I directional coupler. In addition, the directivity of the ESICL III directional coupler at $f_0 = 5$ GHz is higher than 30 dB in the whole band. Therefore, it can be concluded that the simulated performance of the ESICL III directional coupler is better than the other ESICL and microstrip directional couplers.

TABLE 2. Comparison between the proposed directional couplers in this work. Simulated results.

$f_0 = 5$ GHz				
	ESICL I	ESICL II	ESICL III	$\mu Strip$
R_L(dB)	28	26	33	23
I_L (dB)	0.42	0.48	0.48	0.63
I_S (dB)	25	32	40	24
C (dB)	10±0.5	10±0.5	10±0.5	10.2±0.5
FBW_C(%)	34	54	54	59
D (dB)	11	22	30	13
$f_0 = 15$ GHz				
	ESICL I	ESICL II	ESICL III	$\mu Strip$
R_L(dB)	26	23	28	20
I_L (dB)	0.57	0.48	0.48	0.58
I_S (dB)	15	24	34	21
C (dB)	10±0.5	10±0.5	10±0.5	10.0±0.5
FBW_C(%)	50	55	55	50
D (dB)	0	10	24	12.5

B. FABRICATION AND MEASUREMENTS OF THE DIRECTIONAL COUPLERS

Prototypes of the proposed ESICL directional coupler have been fabricated and measured at two frequencies, $f_0 = 5$ GHz and $f_0 = 15$ GHz, to verify the feasibility of the solution. Additionally, microstrip directional couplers at the same frequencies were manufactured and measured to facilitate a comparison with the ESICL prototypes. Standard PCB manufacturing processes have been used for all the implemented prototypes. For the ESICL directional couplers, ROGERS 4003C substrate with a permittivity constant of $\epsilon_r = 3.55$ and a height of $h_s = 0.813$ for all layers have been used. In the case of the microstrip directional coupler at the $f_0 = 5$ GHz frequency, the same substrate and height were utilized. However, for the $f_0 = 15$ GHz frequency, the same substrate type with a height of $h_s = 0.305$ mm has been used. Fig. 17a) shows the ESICL directional coupler without assembly, and Figure 17b) highlights the most important details of the central layer. The assembled prototype is presented in Fig. 17c). Four GCPW-to-ESICL transitions [19] and lines of GCPW have been utilized for measurement, with the ESICL extended to properly connect the SMA connectors. Furthermore, Fig. 17d) shows the microstrip directional couplers. A thru-reflect-line (TRL) de-embedding calibration kit has been fabricated for the input GCPW and microstrips, as depicted in Fig. 17e). The reference planes in the prototypes were marked in blue color. The purpose of

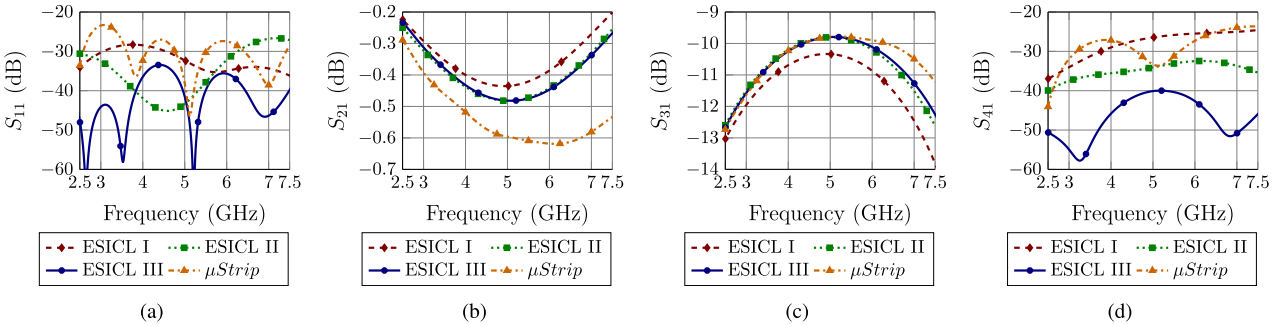

FIGURE 12. Simulated performance of ESICL I, ESICL II and ESICL III directional couplers at operation frequency ($f_0 = 5$ GHz) for $C = 10$ dB and comparison with conventional microstrip directional coupler with the same specifications. (a) Reflection coefficient S_{11}. (b) Transmission coefficient S_{21}. (c) Coupling coefficient S_{31}. (d) Isolation coefficient S_{41}.

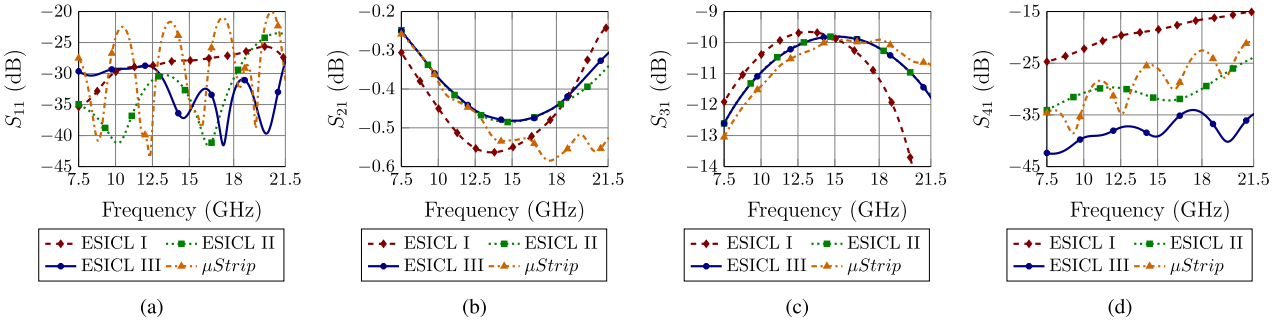

FIGURE 13. Simulated performance of ESICL I, ESICL II and ESICL III directional couplers at operation frequency ($f_0 = 15$ Ghz) for $C = 10$ dB and comparison with conventional microstrip directional coupler with the same specifications. (a) Reflection coefficient S_{11}. (b) Transmission coefficient S_{21}. (c) Coupling coefficient S_{31}. (d) Isolation coefficient S_{41}.

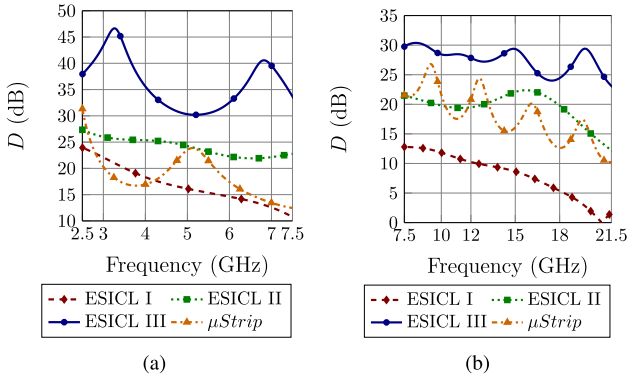

FIGURE 14. Simulated directivity of ESICL I, ESICL II, ESICL III and microstrip directional couplers at operation frequency of (a) $f_0 = 5$ GHz, (b) $f_0 = 15$ GHz.

this TRL is to eliminate the insertion loss from the coaxial connectors and the GCPW/microstrip lines.

The Keysight N5245A VNA was used to measure all the manufactured prototypes. Fig. 15 shows the comparison between simulation and measurement results of the ESICL and microstrip directional couplers for an operation frequency of $f_0 = 5$ GHz, whereas for an operation frequency of $f_0 = 15$ GHz results are shown in Fig. 16. The measured results partially align with the simulated results; more agreement between both (simulations and measurements) is obtained for the directional coupler at operation frequency $f_0 = 5$ GHz, instead of the directional coupler at $f_0 = 15$ GHz. The differences between simulations and measurements are due to the fabrication tolerances and transitions, which degraded the overall performance of the ESICL directional couplers. The laser beam tolerance for cutting the substrate is 2 μm within the same cut. However, when it comes to aligning the layers and repositioning the laser beam for non-consecutive cuts, the tolerance increases to approximately 50 μm.

The comparison between simulated and measured directivity for both frequencies is shown in Fig. 18. Table 3 summarizes the results of the directional couplers in this work in several indexes, such as minimum level of return losses R_L (dB) and fractional bandwidth FBW_{R_L} (%), the maximum value of insertion losses I_L (dB), the minimum value of isolation I_S (dB), coupling coefficient C (dB), minimum value of directivity D (dB) in the whole frequency band, fractional bandwidth FBW_D (%) of this minimum value, and D (dB) at operation frequency. It can be observed that lower insertion losses have been attained in ESICL directional couplers when compared to their microstrip counterparts. The ESICL directional coupler exhibits a robust measured coupling performance at $f_0 = 5$ GHz, with a coupling coefficient C of 10.32 dB at the operational frequency, and a consistent range of 10.32 ± 0.5 dB from 4.03 to 6.12 GHz,

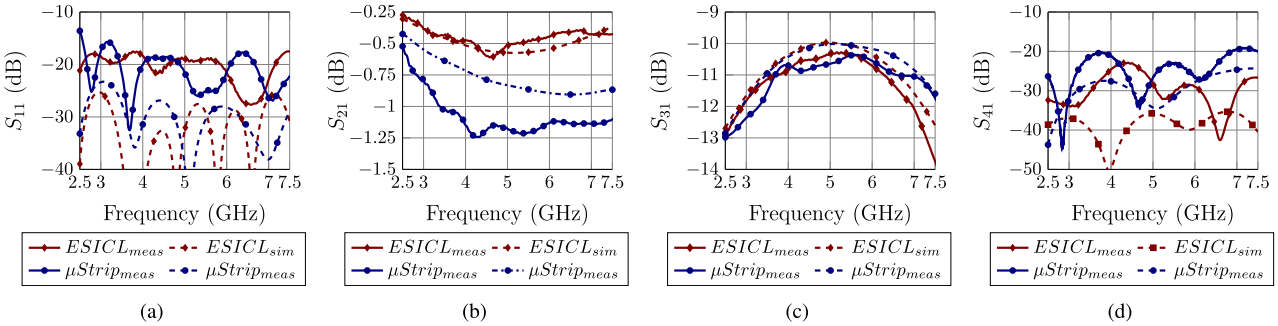

FIGURE 15. Simulated and measured comparison between ESICL III and microstrip directional couplers at operation frequency ($f_0 = 5$ GHz) for $C = 10$ dB. (a) Reflection coefficient S_{11}. (b) Transmission coefficient S_{21}. (c) Coupling coefficient S_{31}. (d) Isolation coefficient S_{41}.

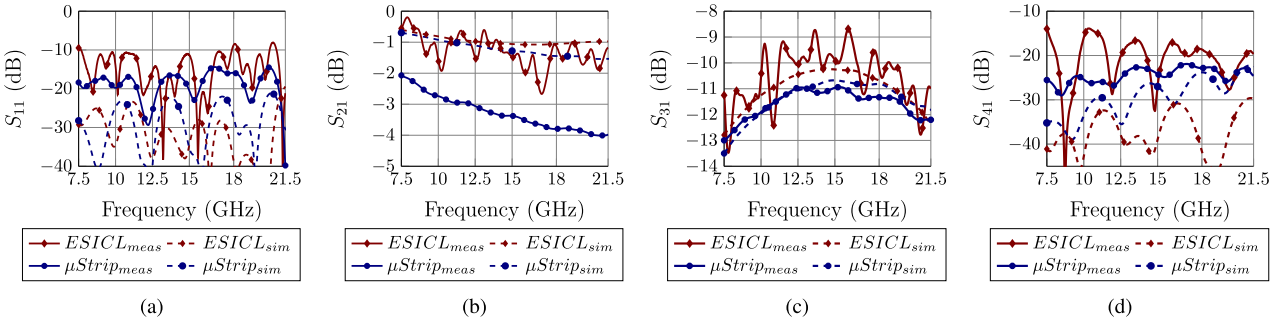

FIGURE 16. Simulated and measured comparison between ESICL III and microstrip directional couplers at operation frequency ($f_0 = 15$ GHz) for $C = 10$ dB. (a) Reflection coefficient S_{11}. (b) Transmission coefficient S_{21}. (c) Coupling coefficient S_{31}. (d) Isolation coefficient S_{41}.

TABLE 3. Comparison between the proposed direction couplers and previous reported.

	[16]	[35]	[36]	[7]	This Work	This Work	This Work	This work
Technology	SICL	$\mu Strip$	Coaxial	$\mu Strip$	ESICL	ESICL	$\mu Strip$	$\mu Strip$
f_0	2.35	2	N.R	2.4	5	15	5	15
R_L(dB)	22	20	20	20**	33*/17.5	28*/10	23*/17.5	20*/15
$FBW_{R_L}(\%)$	69	29	196	20**	100*/100	96*/96	100*/48	96*/96
I_L (dB)	N.R	N.R	1.33	N.R	0.48*/0.6	0.48*/2.6	0.63*/1.25	0.58*/4
I_S (dB)	32	N.R	28**	N.R	40*/23	34*/14	24*/19	21*/22
$C(f_0)$ (dB)	20	10	17	20	10*/10.32	10*/9.88	10.2*/10.64	10*/10.96
Minimum D (dB)	15**	28.7	10	20	30*/12	24*/13	13*/8	12.5*/11
$FBW_D(\%)$	105	29	196	16.3	100*/100	100*/100	100*/100	100*/100
$D(f_0)$ (dB)	18**	40*	N.R	56	30*/18	29*/23	23*/16	16*/13
Manufact. Complexity	Simple	High	High	High	Simple	Simple	Simple	Simple

*Simulated results without transitions
**Estimated results of the graph
N.R: Not reported

corresponding to an $FBW = 42\%$. Conversely, the microstrip directional coupler yields a coupling coefficient of $C = 10.64$ dB at $f_0 = 5$ GHz, which is furthest from the design parameter value.

The directivity of the ESICL directional coupler at $f_0 = 5$ GHz is 4 dB greater than that of the microstrip coupler in the same frequency band. Notably, the directivity of the ESICL directional coupler appears to be more stable than that of the microstrip directional coupler. Regarding to the $f_0 = 15$ GHz ESICL directional coupler, some ripples in the coupling coefficient are observed due to manufacturing tolerances. Nonetheless, at operation frequency, the coupling coefficient is $C = 9.88$ dB, while the microstrip directional coupler registers a value of 10.96 dB. These are differences of 0.12 dB and 0.96 dB from their respective design values. In the realm of directivity, the ESICL directional coupler showcases a directivity value of $D = 23$ dB at the operation frequency, while the microstrip coupler shows a directivity of $D = 13$ dB, which is a difference of 10 dB. Consequently, the ESICL directional coupler outperforms its microstrip counterpart in terms of directivity.

C. ANALYSIS AND DISCUSSION OF RESULTS

Several directional coupler configurations have been designed and measured using ESICL and microstrip technologies. Table 3 compares the performance of the

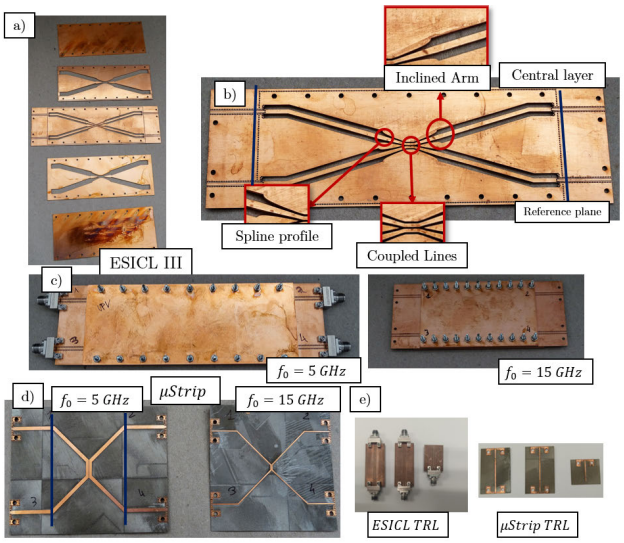

FIGURE 17. Photographs of the manufactured prototype directional couplers. (a) ESICL directional coupler prior to assembly. (b) Central layer of ESICL directional coupler with key details marked. The reference plane for the calibration kit is marked in blue. c) Assembled ESICL directional coupler. d) Microstrip directional coupler. The reference plane for the calibration kit is marked in blue. e) Microstrip and CPW TRL calibration kits.

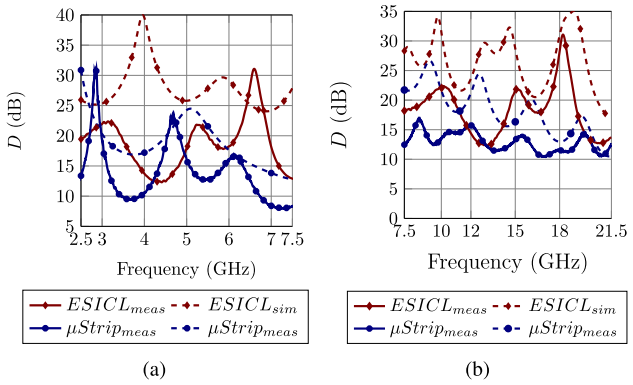

FIGURE 18. Simulated and measured directivity comparison between ESICL III and microstrip directional coupler at operation frequency of (a) $f_0 = 5$ GHz, (b) $f_0 = 15$ GHz.

proposed directional couplers (with both measured and simulated data) with several previously designed directional couplers in alternative technologies. It is evident that the proposed ESICL directional couplers exhibit lower losses and improved directivity when compared to the microstrip directional couplers presented in this paper. Furthermore, it should be noted that in the ESICL couplers, due to the transition, their response is degraded (return losses and directivity), but it is still better, including this situation. It is noteworthy that the underlying concept in the ESICL involves the comprehensive development of all microwave components within this low-loss line, minimizing transitions to the necessary minimum. In comparison to the SICL-reported solution [16], the proposed directional coupler delivers comparable performance while operating at a higher frequency. The reported microstrip-based solutions [7], [35] offer superior directivity, but require the use of lumped elements or complex structures, resulting in more complex fabrication that becomes increasingly challenging at higher frequencies. Furthermore, the same concept of incorporating lumped elements can be applied to the directional coupler, as reported in [24], with a Wilkinson divider.

V. CONCLUSION

In this paper, several directional couplers using ESICL technology have been designed and implemented. An evolution of the ESICL directional coupler has been explained, beginning with one featuring 90-degree bends, progressing to a coupler with inclined arms and a high isolation section, and culminating in the finally proposed directional coupler based on inclined arms, a high isolation section, and a spline transition. The inclined arms and high-isolation sections enhance the isolation, while the spline transition ensures improved matching between the access lines and the high-isolation section. A comprehensive study of the design parameters that rule the directional coupler performance has been conducted and a design procedure has been presented. Subsequently, two examples have been designed and manufactured at operation frequencies of $f_0 = 5$ GHz, and $f_0 = 15$ GHz, for a coupling coefficient of $C = 10$ dB in ESICL technology. Both directional couplers present simulated return losses better than 28 dB, insertion losses below 0.5 dB, and directivity better than 24 dB in the whole band. To compare, microstrip directional couplers with the same coupling coefficient have also been designed and manufactured. The measurements of the prototype responses prove that the ESICL provides lower losses and high directivity. Consequently, the results clearly indicate that ESICL directional couplers outperform their microstrip counterparts. Hence, it is substantiated that ESICL technology can be a strong option for applications with substantial requirements in terms of weight, size, loss, and integrability.

REFERENCES

[1] A. Tasić, W. A. Serdijn, L. E. Larson, and G. Setti, *Circuits and Systems for Future Generations of Wireless Communications*. Berlin, Germany: Springer, 2009.

[2] V. Boria and B. Gimeno, "Waveguide filters for satellites," *IEEE Microw. Mag.*, vol. 8, no. 5, pp. 60–70, Oct. 2007.

[3] A. Belenguer, A. L. Borja, H. Esteban, and V. E. Boria, "High-performance coplanar waveguide to empty substrate integrated coaxial line transition," *IEEE Trans. Microw. Theory Techn.*, vol. 63, no. 12, pp. 4027–4034, Dec. 2015.

[4] E. A. Wolff and R. Kaul, *Microwave Engineering and Systems Applications*. New York, NY, USA: Wiley, 1988.

[5] S. L. March, "Phase velocity compensation in parallel-coupled microstrip," in *IEEE MTT-S Int. Microw. Symp. Dig.*, Jun. 1982, pp. 410–412.

[6] S. Lee and Y. Lee, "An inductor-loaded microstrip directional coupler for directivity enhancement," *IEEE Microw. Wireless Compon. Lett.*, vol. 19, no. 6, pp. 362–364, Jun. 2009.

[7] S. Lee and Y. Lee, "A design method for microstrip directional couplers loaded with shunt inductors for directivity enhancement," *IEEE Trans. Microw. Theory Techn.*, vol. 58, no. 4, pp. 994–1002, Apr. 2010.

[8] D. Jaisson, "Multilayer microstrip directional coupler with discrete coupling," *IEEE Trans. Microw. Theory Techn.*, vol. 48, no. 9, pp. 1591–1595, Sep. 2000.

[9] Z.-Q. Wang, M.-J. Zheng, Y.-B. Fu, and F. Xiao, "A design of 3-dB wiggly line coupler using micromachining technology and compared with 3-dB Lange coupler," in *Proc. Int. Workshop Anti-Counterfeiting, Secur. Identificat. (ASID)*, 2007, pp. 48–51.

[10] F. Gatti, M. Bozzi, L. Perregrini, K. Wu, and R. G. Bosisio, "A novel substrate integrated coaxial line (SICL) for wide-band applications," in *Proc. Eur. Microw. Conf.*, Sep. 2006, pp. 1614–1617.

[11] K. Fan, X. Fan, Q. Tan, F. Zhu, Y. Yu, and G. Q. Luo, "SICL-fed balanced antipodal dipole antenna with wideband operation and cross-polarization improvement at millimeter-wave band," *IEEE Antennas Wireless Propag. Lett.*, vol. 22, pp. 447–451, 2023.

[12] F.-F. Fan, Q.-L. Chen, Y.-X. Xu, X.-F. Zhao, J.-C. Feng, and Z.-H. Yan, "A wideband compact printed dipole antenna array with SICL feeding network for 5G application," *IEEE Antennas Wireless Propag. Lett.*, vol. 22, pp. 283–287, 2023.

[13] Y. Wei, C. Arnold, and J. Hong, "A K/Ka-band reconfigurable substrate integrated coaxial line to waveguide transition technology," *IEEE Access*, vol. 10, pp. 65037–65043, 2022.

[14] M. Cariou, B. Potelon, C. Quendo, S. Cadiou, E. Schlaffer, W. Pessl, and A. Le Fevre, "Compact X-band filter based on substrate integrated coaxial line stubs using advanced multilayer PCB technology," *IEEE Trans. Microw. Theory Techn.*, vol. 65, no. 2, pp. 496–503, Feb. 2017.

[15] G.-W. Su, Y.-L. Shen, W. Hong, and M.-H. Ho, "Wide-band directional coupler design using the substrate integrated double-strip coaxial line," in *Proc. IEEE Asia–Pacific Microw. Conf. (APMC)*, Dec. 2019, pp. 1011–1013.

[16] S. Jun-Yu, L. Qiang, W. Yong-Le, L. Yuan-An, L. Shu-Lan, Y. Cui-Ping, and L. Gan, "High-directivity single- and dual-band directional couplers based on substrate integrated coaxial line technology," in *IEEE MTT-S Int. Microw. Symp. Dig.*, Jun. 2013, pp. 1–4.

[17] H. Ranasinghe and A. Gunawardena, "Design of a multi-section coupled line coupler based on substrate integrated coaxial lines," in *Proc. IEEE Int. Conf. Ind. Inf. Syst.*, Dec. 2017, pp. 1–5.

[18] D. Deslandes and K. Wu, "Integrated microstrip and rectangular waveguide in planar form," *IEEE Microw. Wireless Compon. Lett.*, vol. 11, no. 2, pp. 68–70, Feb. 2001.

[19] A. Belenguer, H. Esteban, and V. E. Boria, "Novel empty substrate integrated waveguide for high-performance microwave integrated circuits," *IEEE Trans. Microw. Theory Techn.*, vol. 62, no. 4, pp. 832–839, Apr. 2014.

[20] L. Martinez, A. Belenguer, V. E. Boria, and A. L. Borja, "Compact folded bandpass filter in empty substrate integrated coaxial line at S-band," *IEEE Microw. Wireless Compon. Lett.*, vol. 29, no. 5, pp. 315–317, May 2019.

[21] A. L. Borja, A. Belenguer, H. Esteban, and V. E. Boria, "Design and performance of a high-Q narrow bandwidth bandpass filter in empty substrate integrated coaxial line at Ku-band," *IEEE Microw. Wireless Compon. Lett.*, vol. 27, no. 11, pp. 977–979, Nov. 2017.

[22] A. L. Borja, A. Belenguer, H. Esteban González, and V. E. Boria, "Design procedure of continuous profile stopband filters implemented with empty substrate integrated coaxial lines," *IEEE Trans. Microw. Theory Techn.*, vol. 68, no. 4, pp. 1520–1528, Apr. 2020.

[23] F. Quiles, Á. Belenguer, J. Á. Martínez, V. Nova, H. Esteban, and V. Boria, "Compact microstrip to empty substrate-integrated coaxial line transition," *IEEE Microw. Wireless Compon. Lett.*, vol. 28, no. 12, pp. 1080–1082, Dec. 2018.

[24] J. M. Merello, V. Nova, C. Bachiller, and V. E. Boria, "Compact C-band Wilkinson power divider in empty substrate integrated coaxial line," in *Proc. 51st Eur. Microw. Conf.*, Apr. 2022, pp. 225–228.

[25] J. M. Merello, V. Nova, C. Bachiller, J. R. Sanchez, A. Belenguer, and V. E. B. Esbert, "Miniaturization of power divider and 90° hybrid directional coupler for C-band applications using empty substrate-integrated coaxial lines," *IEEE Trans. Microw. Theory Techn.*, vol. 66, no. 6, pp. 3055–3062, Jun. 2018.

[26] L. Martinez, V. Laur, A. L. Borja, P. Quéffélec, and A. Belenguer, "Low loss ferrite Y-junction circulator based on empty substrate integrated coaxial line at Ku-band," *IEEE Access*, vol. 7, pp. 104789–104796, 2019.

[27] J. Savage, W. Smith, and C. Paul, "Moment method calculation of the per-unit-length parameters of cable bundles," in *Proc. IEEE Symp. Electromagn. Compat.*, Aug. 1994, pp. 441–446.

[28] T.-S. Chen, "Determination of the capacitance, inductance, and characteristic impedance of rectangular lines," *IRE Trans. Microw. Theory Techn.*, vol. 8, no. 5, pp. 510–519, Sep. 1960.

[29] S. Hopfer, "The design of ridged waveguides," *IRE Trans. Microw. Theory Techn.*, vol. 3, no. 5, pp. 20–29, Oct. 1955.

[30] N. Marcuvitz, *Waveguide Handbook*, vol. 21. Edison, NJ, USA: IET, 1951.

[31] D. M. Pozar, *Microwave Engineering*. Hoboken, NJ, USA: Wiley, 2011.

[32] C. De Boor and C. De Boor, *A Practical Guide to Splines*, vol. 27. New York, NY, USA: Springer, 1978.

[33] G. Micula and S. Micula, *Handbook of Splines*, vol. 462. Berlin, Germany: Springer, 2012.

[34] J. Martinez, A. Belenguer, and H. Esteban, "Fast frequency sweep technique based on segmentation for the acceleration of the electromagnetic analysis of microwave devices," *Appl. Sci.*, vol. 9, no. 6, p. 1118, Mar. 2019.

[35] L. Wang, G. Wang, and J. Sidén, "Design of high-directivity wideband microstrip directional coupler with fragment-type structure," *IEEE Trans. Microw. Theory Techn.*, vol. 63, no. 12, pp. 3962–3970, Dec. 2015.

[36] X. Dai, T. Sun, W. Wu, Z. Wang, G. Shi, Q. Yang, C. Guo, and A. Zhang, "A 0.22–26.5-GHz ultra-wideband directional coupler based on copper additive manufacturing," *IEEE Trans. Circuits Syst. II, Exp. Briefs*, vol. 70, no. 8, pp. 2869–2873, Aug. 2023.

DAVID HERRAIZ (Graduate Student Member, IEEE) received the B.Sc. and M.Sc. degrees in telecommunications/electrical engineering and the B.Sc. degree in industrial engineering from Universitat Politècnica de Valencia (UPV), in 2018 and 2020, respectively, where he is currently pursuing the Ph.D. degree in telecommunications engineering.

From 2020 to 2021, he was a Service Engineer with 5G Communications for Future Industry Verticals (Fivecomm), where he played a key role in 5G robotics solutions within several European projects funded under Horizon Europe. His responsibilities included working as a ROS Developer and Applications Integrator with Automated Guided Vehicles (AGVs), as well as handling various project management and execution tasks. In 2021, he joined the Institute of Telecommunications and Multimedia Applications (iTEAM), UPV. Notably, in 2021, he received the Colegio Oficial de Ingenieros de Telecomunicación and Asociación Española de Ingenieros de Telecomunicación (COIT-AEIT) Award in collaboration with HISPASAT, the Spanish Satellite Communications Operator, for his outstanding work on the master's degree final thesis, which focused on emerging technologies for communication satellite payloads. His research interests include wideband transition structures, ridge waveguides, additive manufacturing, and the design, implementation, and optimization of communication devices using empty substrate integrated technologies and their applications.

HÉCTOR ESTEBAN (Senior Member, IEEE) received the degree in telecommunications engineering and the Ph.D. degree from Universidad Politécnica de Valencia (UPV), Spain, in 1996 and 2002, respectively.

He worked with the Joint Research Centre, European Commission, Ispra, Italy. He was with the European Topic Centre on Soil (European Environment Agency), in 1997. He rejoined UPV, in 1998. His research interests include methods for the full-wave analysis of open-space and guided multiple scattering problems, CAD design of microwave devices, electromagnetic characterization of dielectric and magnetic bodies, and the acceleration of electromagnetic analysis methods.

DARÍO HERRAIZ received the bachelor's and master's degrees in telecommunications engineering from Universidad de Castilla-La Mancha (UCLM), Spain, in December 2019 and 2022, respectively, where he is currently pursuing the Ph.D. degree in telecommunications engineering. He joined Grupo de Aplicaciones de Microondas y Milimétricas, y Antenas (GAMMA) Group, UCLM, in 2018, for six months with a research grant, as a Researcher, in 2019 and 2021. His final degree project is about ESIW and was prized with the National Prize from the Colegio Oficial/Asociación de Graduados E Ingenieros Técnicos de Telecomunicación (COITT/AEGITT), in 2020. So far, he has been the coauthor of six articles and the author of one book chapter and one article.

JUAN J. DE DIOS received the Ingeniero de Telecomunicación and Doctor Ingeniero de Telecomunicación (Ph.D.) (summa cum laude) degrees in communications from E.T.S. Ingenieros de Telecomunicación, Universidad Politécnica de Madrid, Spain, in 1991 and 2004, respectively. He was with the Transmission Engineering Laboratory (Bell Labs), Lucent Technologies (formerly AT&T), Madrid, Spain, from 1991 to 1999. Since then, he has been with Escuela Politécnica de Cuenca, Universidad de Castilla-La Mancha, Spain, where he is currently a Profesor Titular de Universidad with Departamento de Ingeniería Eléctrica, Electrónica, Automática y Comunicaciones. He is the author and coauthor of more than 20 publications in international journals and conference proceedings. His research interests include image and video processing, microwave circuits and antennas, and SIW devices analysis and their applications. He acted as a reviewer for four international publications.

MARCOS D. FERNANDEZ received the degree in telecommunications engineering from Universitat Politècnica de Catalunya (UPC), Spain, in 1996, and the Ph.D. degree from Universidad Politécnica de Madrid (UPM), in 2006. He joined Universidad de Castilla-La Mancha, in 2000, where he is currently a Profesor Titular de Universidad with Departamento de Ingeniería Eléctrica, Electrónica, Automática y Comunicaciones, and the Dean of Escuela Politécnica de Cuenca. He has authored or coauthored more than 60 papers in peer-reviewed international journals and conference proceedings. His research interests include empty substrate integrated waveguide (ESIW, ESICL) devices, empty patch antennas, and their manufacturing and applications.

ANGEL BELENGUER (Senior Member, IEEE) received the degree in telecommunications engineering and the Ph.D. degree from Universitat Politècnica de València (UPV), Spain, in 2000 and 2009, respectively. He joined Universidad de Castilla-La Mancha, in 2000, where he is currently a Catedrático de Universidad with Departamento de Ingeniería Eléctrica, Electrónica, Automática y Comunicaciones. He has authored or coauthored more than 90 papers in peer-reviewed international journals and conference proceedings and frequently acts as a reviewer for several international technical publications. His research interests include methods in the frequency domain for the full-wave analysis of microwave passive devices, and substrate integrated waveguide (SIW) and empty substrate integrated waveguide (ESIW) devices and their applications.

VICENTE E. BORIA (Fellow, IEEE) was born in Valencia, Spain, in May 1970. He received the Ingeniero de Telecomunicación (Hons.) and Doctor Ingeniero de Telecomunicación degrees from Universidad Politécnica de Valencia, Valencia, in 1993 and 1997, respectively.

In 1993, he joined Departamento de Comunicaciones, Universidad Politécnica de Valencia, where he has been a Full Professor, since 2003. In 1995 and 1996, he held a Spanish Trainee Position with the European Space Research and Technology Centre, European Space Agency (ESTEC-ESA), Noordwijk, The Netherlands, where he was involved in the area of EM analysis and design of passive waveguide devices. He has authored or coauthored 15 chapters in technical textbooks, 200 articles in refereed international technical journals, and over 250 papers in international conference proceedings. His current research interests include the analysis and automated design of passive components (in particular filters and multiplexers) in several technologies and the simulation and measurement of power effects in high-frequency devices and systems.

Dr. Boria has been a member of the IEEE Microwave Theory and Techniques Society (IEEE MTT-S) and the IEEE Antennas and Propagation Society (IEEE AP-S), since 1992. He is a member of the European Microwave Association (EuMA) and has been the Chair of the 48th European Microwave Conference, Madrid, Spain. He is also a member of the Technical Committees of the IEEE-MTT International Microwave Symposium and of the European Microwave Conference. He acts as a regular reviewer of the most relevant IEEE and IET technical journals on his areas of interest. He has been an Associate Editor of IEEE Microwave and Wireless Components Letters, from 2013 to 2018, and *IET Electronics Letters*, from 2015 to 2018. Presently, he serves as a Subject Editor (Microwaves) for *IET Electronics Letters* and an Editorial Board Member for *International Journal of RF and Microwave Computer-Aided Engineering*.